Phase Behavior of Block Copolymer/Homopolymer Blends

M. W. Matsen

Department of Chemical Engineering and Materials Science, University of Minnesota, Minneapolis, Minnesota 55455

Received April 4, 1995; Revised Manuscript Received May 26, 1995[⊗]

ABSTRACT: We examine weakly segregated blends of AB diblock copolymer and A homopolymer with similar degrees of polymerization. The relative stability of numerous phases is examined and phase diagrams are constructed using self-consistent field theory. While the pure diblock system is only found to exhibit the body-centered cubic (spherical), hexagonal (cylindrical), bicontinuous $Ia\bar{3}d$ cubic (gyroid), and lamellar ordered phases, we find that the addition of homopolymer stabilizes close-packed spherical, bicontinuous $Pn\bar{3}m$ cubic (double-diamond), and hexagonally-perforated (catenoid) lamellar phases. We find that, in general, the minority-component region of a microstructure can only accommodate a limited amount of homopolymer before macrophase separation occurs. On the other hand, the majority-component regions can swell indefinitely with the addition of homopolymer, eventually resulting in an unbinding transition. We associate the region of highly-swollen microstructures with the micellar region observed in real systems. For the lamellar and hexagonal phases, we examine the distribution of homopolymer within the microstructure, and for the lamellar phase, we calculate the effect of homopolymer on the dimensions of the A- and B-rich microdomains.

1. Introduction

The self-assembly of block copolymer molecules into various and often elaborate microstructures has attracted considerable attention. Much of this interest stems from the fact that copolymers exhibit structures like those observed in other "soft material" systems involving, for instance, lipids,[1-3] surfactants,[4] and liquid crystals.[5] Furthermore, similar structures are observed in complex biological systems.[1,6] Generally, the mechanisms responsible for molecular self-assembly are easily understood, while those that determine the geometry of the resulting structures are not so easily understood. The mechanisms involved will differ somewhat from system to system. In pure diblock copolymer melts, the factors dictating geometry are, to a large degree, explained.[7] However, for multicomponent copolymer blends, the understanding is rather incomplete, indicating a need for further study. Because diblock/homopolymer melts are among the simplest blends, as well as being closely analogous to other two-component self-assembling systems such as lipid/water ones, they are a natural system for a more thorough study.

The physics governing the microphase separation of pure AB diblock melts is straightforward. At high temperatures, the system forms a disordered (DIS) phase so as to maximize entropy. As the temperature is lowered or the degree of polymerization increased, the A and B blocks of the copolymer will separate, provided they are immiscible (*i.e.*, if the Flory–Huggins parameter, χ, is positive). However, the connectivity of the immiscible blocks prevents macrophase separation, and instead, a structure forms with microscopic-sized A- and B-rich regions separated by an extensive amount of internal interface. The length scale of this microstructure is determined by a competition between the interfacial tension, which favors large domain sizes, and the entropic stretching energy of the polymer, which prefers small domains. The stretching occurs due to the incompressibility of the melt enforcing the overall monomer density to be uniform.

The geometry of the structure that forms is determined to a large extent by the competition between the A and B blocks as to which will have to stretch the most. When both have comparable degrees of polymerization, the competition is balanced and flat interfaces occur. However, when one block has a greater degree of polymerization, the system prefers to form curved interfaces with the larger block on the convex side and the smaller one on the concave side. For a fixed interfacial area per copolymer, this allows the large block to relax while the small one must stretch. However, the cost of stretching the small block is more than compensated for by the relaxation of the large one, and hence, the overall entropic stretching energy is reduced. This accounts for the progression of the minority-component domains from flat lamellae to cylinders to spheres as the asymmetry between the A and B blocks is increased producing a larger spontaneous mean curvature. We note that this progression is also influenced by asymmetry in the A- and B-monomer statistical segment lengths.[7,8]

The above units form the "classical" phases: the lamellar (L) structure, the hexagonally (H) arranged cylinders, and the body-centered cubic ($Q_{Im\bar{3}m}$) ordered spheres. It is now clear that between the L and H phases a number of other structures compete for stability.[7] In order to be stable, the structure not only should have an interface with a curvature that nowhere deviates significantly from the spontaneous curvature but also should allow the molecules to pack efficiently. Within some structures, there will be regions requiring polymers to stretch excessively in order to maintain a constant monomer density, and these are unlikely to be stable. It is difficult to determine which structures minimize these stressed regions while providing the desired interfacial curvature. For some time, it was thought that the bicontinuous $Pn\bar{3}m$ cubic ($Q_{Pn\bar{3}m}$) phase, often referred to as the double-diamond phase, was one.[9] In this phase, the minority component forms two interweaving diamond lattices with the majority component filling the space between them. More recent experiments have cast doubts on this[10] and suggest that the actual structure observed was a bicontinuous $Ia\bar{3}d$ cubic ($Q_{Ia\bar{3}d}$) phase,[11] sometimes referred to as the gyroid phase. This structure is very similar except that the minority component forms two 3-fold-coordinated lat-

[⊗] Abstract published in *Advance ACS Abstracts,* July 15, 1995.

0024-9297/95/2228-5765$09.00/0

tices rather than diamond ones which are 4-fold coordinated. Also observed is a hexagonally-perforated lamellar (HPL) phase,[7,12] sometimes called the catenoid lamellar phase, where minority-component lamellae are perforated by a hexagonal arrangement of holes. The holes between adjacent minority-component lamellae are staggered, but it is still unknown whether these lamellae pack in an abab... or an abcabc... sequence.

The addition of A homopolymer to the melt provides new behavior. For instance, the presence of a second component leads to macrophase separation, *i.e.*, biphasic regions. Furthermore, it allows the A-rich regions to swell to macroscopic sizes while the B-rich regions remain as microscopic micelles. A more subtle effect of the homopolymer is to alleviate stress in the A blocks of the copolymer by occupying regions in the microstructure that otherwise would be filled by highly stretched copolymers. Because this will affect different phases to varying degrees, it can alter their relative stabilities and bring about new equilibrium structures.[13,14] This is particularly true between the L and H phases where there is a close competition involving the $Q_{Pn\bar{3}m}$, $Q_{Ia\bar{3}d}$, and HPL phases. Also, in the case of the $Q_{Im\bar{3}m}$ phase, there is evidence that alleviating these stresses allows the bcc ordered spheres to rearrange into a close-packed spherical (CPS) phase[13-16] or a simple cubic one.[17,18] Another equally important consequence of the homopolymer is its effect on the spontaneous curvature of the internal interface, which, in turn, can produce phase transitions between different microstructures. This occurs because the entropy of mixing causes the homopolymer to swell the A blocks of the copolymer, curving the interface toward the B-rich domains.

Considering all the effects in diblock/homopolymer blends, there is much that remains to be studied. Past research has focused on a few issues such as the distribution of homopolymer in the lamellar microstructure[19-24] and the micellar region.[15,17,19,25-28] Still, little has been done to establish the global phase behavior. Experimentally, a number of samples have been examined and the phases they exhibit identified.[18,21,22,29-32] Observed are the ordered L, H, $Q_{Im\bar{3}m}$, $Q_{Pn\bar{3}m}$, $Q_{Ia\bar{3}d}$, and HPL phases[33] and a disordered phase with various micellar regions. Early attempts to determine phase behavior correlated microstructures with the overall A-monomer volume fraction,[18,20] which is inappropriate since the effects of adding A homopolymer are much different than those of adding A monomers to the copolymer. However, as of yet, too few samples have been examined to begin constructing proper experimental phase diagrams. On the theoretical side, Whitmore and Noolandi[34] have examined the interplay between microphase and macrophase separation in the weak-segregation limit. However, their study only considered the lamellar morphology. There are now calculations which examine numerous ordered structures, one for strongly segregated melts[13] and another for weakly segregated ones.[14]

In this paper, we extend our previous work,[14] which used self-consistent field theory (SCFT)[35,36] to examine weakly segregated blends of AB diblock copolymer and A homopolymer. Before beginning our calculation, we recast the equations of the SCFT from the real-space representation in ref 14 to the more convenient basis-function representation in ref 37. We then start by considering blends containing nearly symmetric diblocks and examine the solubility of homopolymer in the lamellar morphology. We find that large homopolymers tend to be immiscible with the microstructure and hence phase separate, whereas small ones tend to be miscible and can swell the microstructure, causing the lattice spacing to diverge. Recognizing that fluctuations, not considered in the SCFT, would cause highly swollen structures to disorder, we associate them with the experimentally observed micellar regions. Next, slices through the phase diagram are calculated for various degrees of segregation and homopolymer molecular weights. In these slices, all the phases discussed in this section are considered, and regions of stability are found for the L, H, $Q_{Im\bar{3}m}$, $Q_{Ia\bar{3}d}$, $Q_{Pn\bar{3}m}$, HPL, and CPS ordered phases. We conclude our study by examining the homopolymer distribution within the lamellar and hexagonal phases. Understanding the factors that control this distribution leads to simple physical explanations for the behavior predicted by our calculations.

2. Theory

We consider binary blends of AB diblock copolymer and A homopolymer. The A and B blocks of each copolymer molecule consist of fN and $(1 - f)N$ monomers, respectively, while each homopolymer molecule possesses αN monomers. We assume that all monomers are incompressible and define them such that they each occupy a volume, $1/\rho_0$. In this paper, it is assumed that both monomer types have the same statistical segment length, a.[38] The immiscibility between A and B monomers is controlled by the Flory–Huggins parameter, χ.

In an earlier paper,[14] we demonstrated a straightforward way of formulating the self-consistent field theory (SCFT) for multicomponent polymer systems[41] in the grand-canonical ensemble. There, the equations were expressed in their real-space representation. Below, we express them in an orthonormal-basis-function representation, which is more convenient when dealing with the ordered periodic phases these systems exhibit. The basis functions, $f_i(\mathbf{r})$, allow us to express a given function, $g(\mathbf{r})$, as

$$g(\mathbf{r}) = \sum_i g_i f_i(\mathbf{r}) \tag{1}$$

where

$$\frac{1}{V}\int_V \mathrm{d}\mathbf{r}\, f_i(\mathbf{r})\, f_j(\mathbf{r}) = \delta_{ij} \tag{2}$$

which then permit us to represent $g(\mathbf{r})$ in terms of the amplitudes, g_i. The series, $f_i(\mathbf{r})$, will only include functions that first possess the symmetry of the phase being considered and secondly are eigenfunctions of the Laplacian operator,

$$\nabla^2 f_i(\mathbf{r}) = -\frac{\lambda_i}{D^2} f_i(\mathbf{r}) \tag{3}$$

where D is some length scale for the periodic phase. We order the functions starting with $f_1(\mathbf{r}) = 1$ such that λ_i is a nondecreasing series. For the lamellar phase, we use $f_i(\mathbf{r}) = \sqrt{2}\cos(2\pi(i-1)z/D)$ with $\lambda_i = 4\pi^2(i-1)^2$ for $i \geq 2$, where z is the coordinate orthogonal to the lamellae. Basis functions are provided in ref 39 for the phases with other space-group symmetries.[40] Typically, each λ_i is a constant, but for phases that involve two independent length scales such as the HPL one, it depends on the ratio of the two lengths.

The first step in the SCFT is to solve for a noninteracting system of polymers subject to fields, $w_A(\mathbf{r})$ and $w_B(\mathbf{r})$, which act on A and B monomers, respectively. In this noninteracting system, we are able to calculate the average A- and B-monomer densities, $\phi_A(\mathbf{r})$ and $\phi_B(\mathbf{r})$, respectively. The next step involves adjusting $w_A(\mathbf{r})$ and $w_B(\mathbf{r})$ in order to satisfy the self-consistent field equations,

$$\chi N(\phi_{A,i} - \phi_{B,i}) = \omega_{B,i} - \omega_{A,i} \qquad \text{for } i = 1, 2, 3, \ldots \quad (4)$$

$$\phi_{A,i} + \phi_{B,i} = \delta_{i1} \qquad \text{for } i = 1, 2, 3, \ldots \quad (5)$$

The amplitudes of $\phi_A(\mathbf{r})$ and of $\phi_B(\mathbf{r})$ are given by

$$\phi_{A,i} = \sum_{jk} \Gamma_{ijk}\{\int_0^f ds\, q_{c,j}(s)\, q^\dagger_{c,k}(s) + z\int_0^\alpha ds\, q_{h,j}(s)\, q_{h,k}(\alpha - s)\} \quad (6)$$

$$\phi_{B,i} = \sum_{jk} \Gamma_{ijk} \int_f^1 ds\, q_{c,j}(s)\, q^\dagger_{c,k}(s) \quad (7)$$

where $z = \exp(\mu/k_BT)$, μ is the chemical potential of the homopolymer, and

$$\Gamma_{ijk} = \frac{1}{V}\int_V d\mathbf{r}\, f_i(\mathbf{r})\, f_j(\mathbf{r})\, f_k(\mathbf{r}) \quad (8)$$

The two integrals in eq 6 are the contributions to $\phi_A(\mathbf{r})$ due to A blocks of the copolymer $\phi_{cA}(\mathbf{r})$, and to the homopolymer $\phi_{hA}(\mathbf{r})$, respectively. Above, the amplitudes of the monomer densities are expressed in terms of the amplitudes of end-segment distribution functions

$$q_{c,i}(s) = \begin{cases} \mathbf{T}_{A,i1}(s) & \text{if } s < f \\ \sum_j \mathbf{T}_{B,ij}(s-f)\, \mathbf{T}_{A,j1}(f) & \text{if } f < s \end{cases} \quad (9)$$

$$q^\dagger_{c,i}(s) = \begin{cases} \sum_j \mathbf{T}_{A,ij}(f-s)\, \mathbf{T}_{B,j1}(1-f) & \text{if } s < f \\ \mathbf{T}_{B,i1}(1-s) & \text{if } f < s \end{cases} \quad (10)$$

$$q_{h,i}(s) = \mathbf{T}_{A,i1}(s) \quad (11)$$

which are then expressed in terms of the transfer matrices, $\mathbf{T}_A(s) \equiv \exp(\mathbf{A}s)$ and $\mathbf{T}_B(s) \equiv \exp(\mathbf{B}s)$. The matrix, $\mathbf{A}$, is given by

$$\mathbf{A}_{ij} = -\frac{\lambda_i}{6\Delta^2}\delta_{ij} - \sum_k w_{A,k}\Gamma_{ijk} \quad (12)$$

where $\Delta \equiv D/aN^{1/2}$ is a dimensionless lattice spacing. The matrix, $\mathbf{B}$, is given by a similar expression.

Once the above amplitudes are determined and the self-consistent field equations are satisfied, the free energy or grand-canonical potential, F, is given by

$$\frac{NF}{k_BTQ_0V} = -q_{c,1}(1) - zq_{h,1}(\alpha) + \frac{1}{2}(\chi N - w_{A,1} - w_{B,1}) - \chi N\sum_i \phi_{A,i}\phi_{B,i} \quad (13)$$

For a uniform disordered phase, $\phi_{A,i}$, $\phi_{B,i}$, $w_{A,i}$, and $w_{B,i}$ are all zero for $i \geq 2$, and thus, this expression greatly simplifies. The average volume fraction of the homopolymer, $\phi \equiv \phi_{hA,1}$, is $zq_{h,1}(\alpha) = z\alpha\exp\{-w_{A,1}\alpha\}$, and the volume fraction of the copolymer, $1 - \phi$, is $q_{c,1}(1) = \exp\{-w_{A,1}f - w_{B,1}(1-f)\}$. With this, one can show that for the DIS phase

$$\frac{NF}{k_BTQ_0V} = \frac{\phi}{\alpha}\left(\ln\frac{\phi}{\alpha} - 1\right) + (1-\phi)(\ln(1-\phi) - 1) + \chi N\phi_{A,1}(1-\phi_{A,1}) - \frac{\mu\phi}{\alpha k_BT} \quad (14)$$

where $\phi_{A,1} = \phi + f(1-\phi)$ and

$$\frac{\mu}{\alpha k_BT} = \frac{1}{\alpha}\ln\frac{\phi}{\alpha} - \ln(1-\phi) + \chi N(1-f)(1-2\phi_{A,1}) \quad (15)$$

For a periodic ordered phase, the amplitudes for each quantity form infinite sequences. However, they can be truncated on the basis of an acceptable error tolerance. Our tolerances are generally taken such that the phase boundaries are accurate to within the line widths of our plots. In some cases, this requires up to 200 basis functions. For the periodic phases, the final step is to minimize the free energy with respect to their lattice spacing, D. For the HPL phase, F must also be minimized with respect to the ratio of the lamellar spacing to the spacing of the holes in the perforated layers. By comparing the free energies of different phases, we determine the phase diagram.

3. Results and Discussion

We begin with a calculation analogous to one in ref 34. Here, we are primarily interested in the phase coexistence between homogeneous disordered phases and ordered microstructures. Calculations have shown that the free energy difference between competing microstructures is small compared to that between a microstructure and a disordered phase.[35] Hence, the coexistence region is relatively insensitive to the actual microstructure used in the calculation. Thus, for simplicity, we choose a diblock ($f = 0.45$) that we expect will generally order into the lamellar microstructure and for the moment disregard the possibility of other microstructures. To this particular diblock, we blend three different homopolymers, $\alpha = {}^3/_2$, 1, and ${}^2/_3$. In each case, we calculate the phase diagram as a function of χN and ϕ, where the latter quantity is the volume fraction of the homopolymer. The resulting phase diagrams are shown in Figures 1b, 2b, and 3b.

For small values of χN, the copolymer and homopolymer are completely miscible and they always produce a single homogeneous disordered (DIS) phase. In Figure 1b, where the homopolymer has a polymerization index greater than that of the copolymer ($\alpha = {}^3/_2$), macrophase separation can only occur above the critical point at $\chi N = 5.45$. Above it, the system can separate into homopolymer-rich and diblock-rich DIS phases, but not until $\chi N > 10.38$ does the diblock-rich DIS phase order into the lamellar microstructure. Here, the ordering transition is continuous,[34] but had we considered the other morphologies, presumably, there would be a sequence DIS → $Q_{Im\bar{3}m}$ → H → $Q_{Ia\bar{3}d}$ → L of first-order transitions. The intermediate phases should exist in narrow regions all separated by even narrower coexistence regions. Initially, the solubility of homopolymer in the lamellar phase increases with χN to a maximum of $\phi = 0.109$ and then it decreases, becoming exponentially small in the strong-segregation limit.[13] Decreasing the molecular weight of the homopolymer to $\alpha = 1$

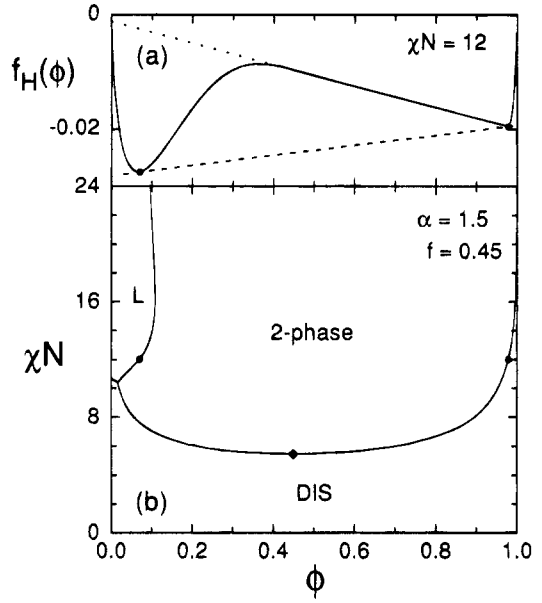

Figure 1. (a) Dimensionless Helmholtz free energy $f_H(\phi)$ as a function of the homopolymer volume fraction ϕ at $\chi N = 12$, $f = 0.45$, and $\alpha = {}^3/_2$. The dashed line shows the double-tangent construction used to locate the binodal points denoted with dots. The dotted line represents the free energy of noninteracting bilayers. (b) Phase diagram obtained by repeating this construction over a range of χN. The dots are the binodal points obtained above, and the diamond denotes a critical point below which two-phase coexistence does not occur.

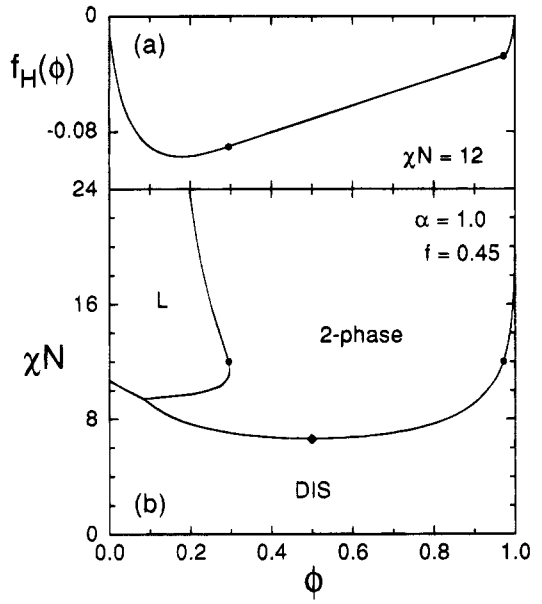

Figure 2. Similar to Figure 1, but for $\alpha = 1$. In (a), the double-tangent construction is not shown for reasons of clarity.

(see Figure 2b) simply reduces the size of the two-phase region. A further reduction (see Figure 3b) can actually lead to the disappearance of the two-phase region. When $\alpha = {}^2/_3$, coexistence between the DIS and L phases occurs only for $\chi N > 18.58$.

To show what happens to the two-phase region, we examine the free energy at $\chi N = 12$ for $\alpha = {}^3/_2$, 1, and ${}^2/_3$. In general, we use the grand-canonical potential to determine phase boundaries, but for illustration purposes, we now consider the Helmholtz potential and perform the double-tangent construction as in ref 34. To proceed, we define a dimensionless Helmholtz free energy, $f_H(\phi) \equiv NF/k_BTQ_0V + \mu\phi/\alpha k_BT + c_1\phi + c_0$, and

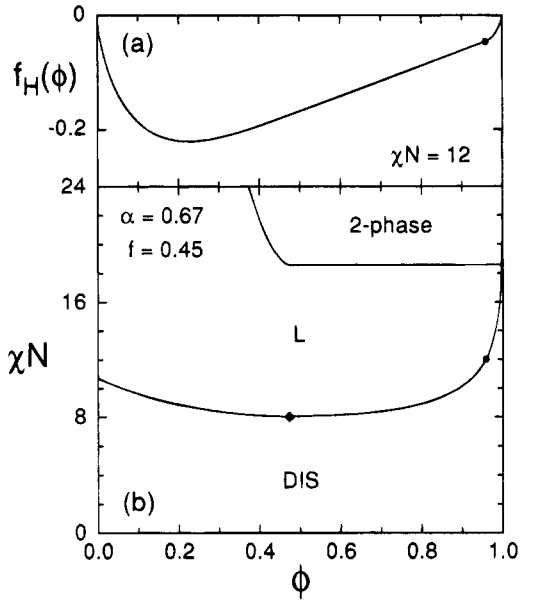

Figure 3. Similar to Figure 1, but for $\alpha = {}^2/_3$. In this case, the free energy curve in (a) does not produce macrophase separation and so the unbinding transition denoted with a dot occurs. In (b), the diamond shows where the stability line for microphase separation meets the unbinding transition.

for reasons of clarity, we choose the arbitrary constants, c_1 and c_0, so that $f_H(0) = f_H(1) = 0$. For the given value of χN, the pure diblock melt ($\phi = 0$) exhibits the lamellar morphology. As ϕ becomes nonzero, the microstructure absorbs homopolymer within the A-rich lamellae causing them to swell. At $\phi \sim 0.4$, the diblocks form bilayers which are well separated by homopolymer. The exceptionally small interaction between bilayers is reflected in the nearly linear dependence of $f_H(\phi)$ on ϕ. Additional homopolymer pushes the bilayers further apart, eventually leading to a continuous unbinding transition where the spacing diverges to infinity, leaving a homopolymer-rich DIS phase. For $\alpha = {}^3/_2$, this occurs at $\phi = 0.9785$. Beyond this point, $f_H(\phi)$ deviates from its nearly linear dependence on ϕ.

The dotted line in Figure 1a tangent to $f_H(\phi)$ in the region of highly swollen lamellae can be interpreted as the free energy of noninteracting bilayers. For $\phi \sim 0.07$, $f_H(\phi)$ drops significantly below this tangent, signifying attractive interactions between the bilayers. This attraction produces a region of negative curvature in $f_H(\phi)$, implying that the system will macrophase separate. The double-tangent construction locates the binodal points at $\phi = 0.0702$ and 0.9792. Since the unbinding transition falls within this interval, it is prevented by the phase separation. The same is true for $\alpha = 1$, but there the attractive interaction is much smaller, and consequently, the negative curvature in the free energy curve is too small to see on the scale of Figure 2a. For that reason, we omit the double-tangent construction and just mark the binodal points with dots. For $\alpha = {}^2/_3$, the bilayers interact repulsively, and thus, a negative curvature in $f_H(\phi)$ does not occur and neither does phase separation. Here, the L and DIS phases are separated by the unbinding transition at $\phi = 0.9591$.

In Figure 3b, the unbinding transition extends from $\chi N = 18.58$ down to 8.03. The weak-segregation limit of this line is denoted with a diamond. As this point is approached from above in the region of highly swollen lamellae, the amplitude of the A-monomer profile across a bilayer becomes zero. Although the lamellar structure becomes weakly segregated, it may still require a large

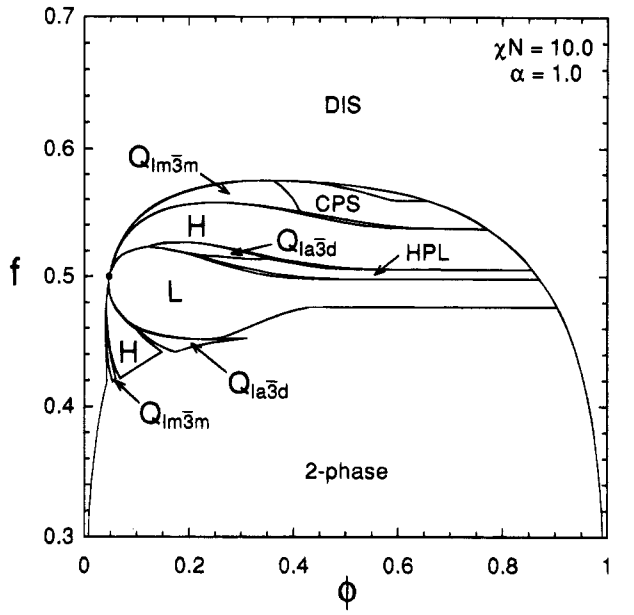

Figure 4. Diblock copolymer/homopolymer phase diagram at $\chi N = 10$ and equal polymerization indices ($\alpha = 1$) plotted in terms of the homopolymer volume fraction ϕ and the A-monomer fraction of the diblock f. For clarity, only the largest biphasic region is labeled.

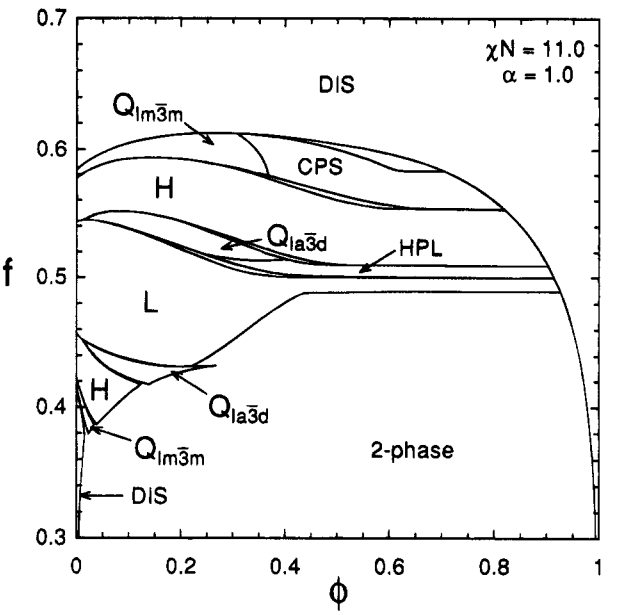

Figure 5. Diblock copolymer/homopolymer phase diagram analogous to that in Figure 4, but at $\chi N = 11$.

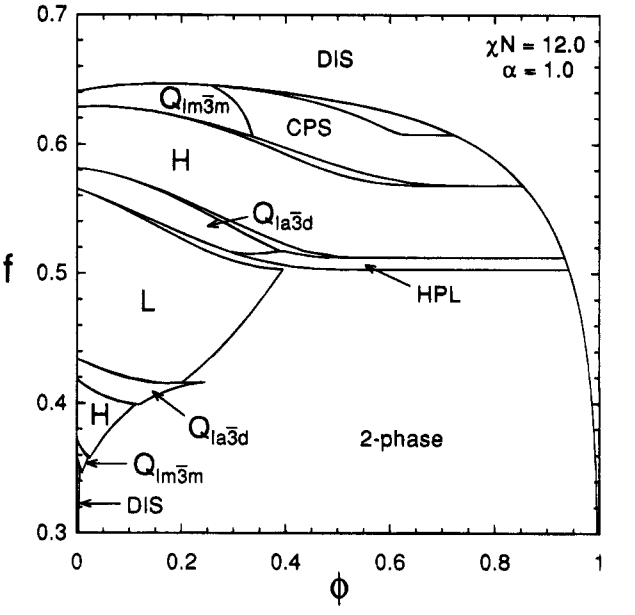

Figure 6. Diblock copolymer/homopolymer phase diagram analogous to that in Figure 4, but at $\chi N = 12$.

number of basis functions to represent the profile accurately. This is because the period of the phase can be much greater than the width of the bilayer, producing a profile which is far from sinusoidal. For this reason, the unbinding transition would be missed using the single-harmonic approximation in refs 34 and 42. We speculate that this is why those references find first-order transitions from one lamellar phase to a second more swollen one, and that, in reality, the lamellar phase swells continuously.

It is important to realize that the stability of the highly swollen lamellar phase is a consequence of the mean-field approximation. Often fluctuations can be ignored in copolymer melts if N is sufficiently large and one is not too close to a mean-field critical point,[43] but here this is not so. Even for $\chi N \approx 18$ and $\alpha = {}^2/_3$, the addition of homopolymer eventually will lead to such weakly ordered bilayers that fluctuations will disorder them, forming a lamellar micellar region prior to the calculated unbinding transition.[19] (Because free edges are energetically unfavorable, we expect these micelles to form closed vesicles.[25]) The micellar region thermodynamically will become part of the DIS phase,[26] and the calculated unbinding transition roughly will correspond to the critical micelle concentration (CMC)[15,17,26,27] where the population of micelles becomes negligible. Because the order–disorder transition between the L phase and the micellar region will be first order,[13,15,17,44] they will be separated by a small coexistence region. As we discuss below, the unbinding of other microstructures also will produce micellar regions, but with different structures.

We now calculate slices through the phase diagram at constant χN and α. Because we examine all values of f including highly asymmetric diblocks, it is unreasonable to limit our consideration of ordered phases to only the lamellar microstructure. For these slices, we consider all the phases discussed in the Introduction. Because of the complexity of some microstructures and high degrees of swelling by the homopolymer, we restrict this study to the weak-segregation regime. Figures 4–6 show the evolution of the phase diagram with increasing χN. Alternatively, the slices in Figures 5, 7, and 8 show the progression of the phase diagram as α decreases at fixed χN. In these figures, we have labeled all the single-phase regions. The biphasic regions separating them are, generally, not labeled and in many cases are too small to be resolved on the scale of the plots.

Each slice of the phase diagram possesses regions of stability for the classical phases, lamellae (L), hexagonally packed cylinders (H), and spheres on a body-center cubic lattice ($Q_{Im\bar{3}m}$). We find that a sufficient amount of homopolymer added to the matrix of the last phase causes the spheres to reorder into a close-packed arrangement, the CPS phase. Such a transition is also predicted for strongly segregated melts.[13] As in the pure diblock melt, the $Q_{Ia\bar{3}d}$ phase is found to be stable between the L and H microstructures.[37] Here, the addition of homopolymer to the matrix of the $Q_{Ia\bar{3}d}$ phase transforms it to the HPL phase. In the other case, when homopolymer is added to the minority-component lat-

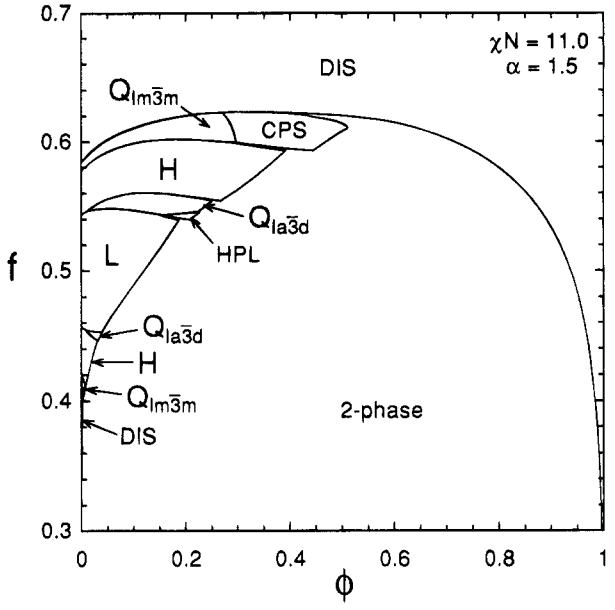

Figure 7. Diblock copolymer/homopolymer phase diagram at $\chi N = 11$ similar to that in Figure 5, but for blends where the homopolymer has a polymerization index greater than that of the diblock ($\alpha = {}^3/_2$).

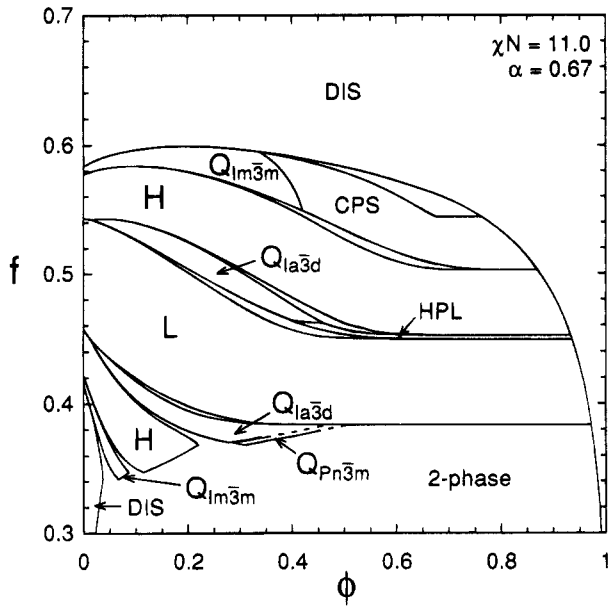

Figure 8. Diblock copolymer/homopolymer phase diagram at $\chi N = 11$ similar to that in Figure 5, but for blends where the homopolymer has a polymerization index less than that of the diblock ($\alpha = {}^2/_3$).

tices of the $Q_{Ia\bar{3}d}$ phase, it can result in a transition to the $Q_{Pn\bar{3}m}$ phase provided the homopolymer has a sufficiently low molecular weight (see Figure 8).

In Figure 7 ($\alpha = {}^3/_2$), the stability of the $Q_{Pn\bar{3}m}$ phase is closest at the DIS + L + $Q_{Ia\bar{3}d}$ triple point. As α decreases, its instability is reduced, eventually producing a DIS + L + $Q_{Ia\bar{3}d}$ + $Q_{Pn\bar{3}m}$ four-phase point at $\alpha = 0.99$. For $\alpha = {}^2/_3$, we find a substantial region of stability for the $Q_{Pn\bar{3}m}$ phase. In Figure 8, we could accurately calculate its phase boundaries only near the H phase. The reason is that it becomes difficult to determine the equilibrium homopolymer concentration, ϕ, in the two bicontinuous cubic phases at the necessary chemical potentials, μ. It was still possible to get accurate values for the free energy, and so we could be confident that the $Q_{Pn\bar{3}m}$ phase completely separates the

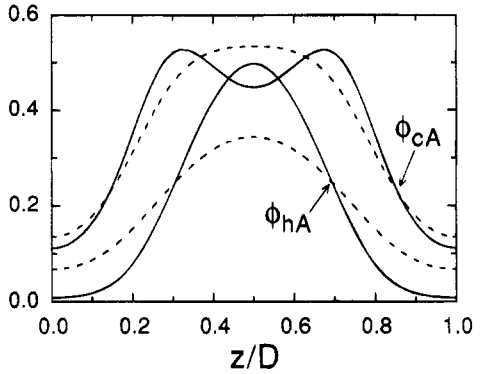

Figure 9. A-monomer profiles in the lamellar phase at $\chi N = 12$, $f = 0.45$, and $\phi = 0.20$ plotted over one period starting from the center of a B-rich lamella. Copolymer and homopolymer contributions, ϕ_{cA} and ϕ_{hA}, respectively, are shown separately. The solid lines correspond to $\alpha = 1$ and the dashed lines to $\alpha = {}^1/_4$.

$Q_{Ia\bar{3}d}$ phase from coexisting with the DIS phase, as indicated by the dashed lines in Figure 8. Notably, this is the situation that occurs in lipid/water systems.[1,2]

For the CPS phase, we have not specified which close-packed arrangement, face-centered cubic (fcc) or hexagonally close-packed (hcp), is favored. This is because we find the two of them to be essentially degenerate in free energy. In the cases where we could distinguish the more stable arrangement, it was the hcp one and the energy difference, $N(\Delta F)/k_B T Q_0 V$, was on the order of 10^{-6}. Likewise, we have not indicated the packing arrangement of the perforated layers in the HPL phase. We examined the sequences, abab... and abcabc..., and found that the two of them are nearly degenerate in free energy. When we can resolve the energy difference, we find that the abab... stacking is favored. For both the CPS and HPL phases, we expect these energy differences to be insignificant in comparison to nonequilibrium effects and suspect that in real blends the stackings will be random. Because ref 21 did not consider this possibility, some doubt exists regarding their claim of bcc spheres at large ϕ. Likewise, such considerations were not explored in ref 17 where a simple cubic (sc) arrangement of spheres was suggested.

Except for the diagram in Figure 4, all the phase diagrams show highly swollen microstructures which unbind continuously upon approaching the DIS phase. As discussed above, these regions will be unstable with respect to fluctuations leading to various micellar regions. The swollen L, H, and CPS phases should disorder into lamellar, cylindrical, and spherical micelles, respectively. Semenov[13] has suggested that the H phase should disorder in two steps, forming a nematic phase prior to the cylindrical micellar region. An analogous sequence could occur for the L phase. Earlier,[14] we suggested that the HPL phase would disorder into disordered struts with most vertices being 3-fold coordinated. Both the HPL phase and the disordered struts have been observed by Disko *et al.*[29] in diblock/homopolymer blends and Hashimoto *et al.*[30] in starblock/homopolymer blends. Han *et al.*[45] present a micrograph of a triblock/homopolymer blend which resembles disordered struts.

As we will demonstrate below, the various effects of adding homopolymer to an ordered diblock melt can be explained by understanding how homopolymer is distributed within the microstructure. For illustration purposes, we consider the lamellar phase. Figure 9 shows the density of A monomers over a complete period

at $\chi N = 12$, $f = 0.45$, and $\phi = 0.20$. The contributions due to the homopolymer $\phi_{hA}(\mathbf{r})$, and due to the copolymer $\phi_{cA}(\mathbf{r})$, are shown separately. The solid lines correspond to $\alpha = 1$ and the dashed lines are for $\alpha = {}^1/_4$. In both cases, the A homopolymer is concentrated toward the center of the A-rich lamellae. The tension in the diblocks coupled with the localization of their junctions to the interface pulls their A monomers toward the interface, expelling the homopolymer toward the center of the lamellae. This is countered by the entropy of mixing which favors a uniform distribution of homopolymer. This entropic effect is enhanced by a lower molecular weight of the homopolymer,[23] and that is why $\phi_{hA}(\mathbf{r})$ has a broader distribution for $\alpha = {}^1/_4$ than for $\alpha = 1$.[21-23]

In Figure 9, the high-weight homopolymer ($\alpha = 1$) forms a well-defined A-rich layer near the middle of the lamella. This layer will produce a field that tends to enhance the order in the adjacent diblock layers, and thus, it increases the degree of segregation. This is how homopolymer manages to induce order in disordered diblock melts at $\chi N = 10$ (see Figure 4). Alternatively, low-weight homopolymer ($\alpha < {}^1/_4$) tends to disorder a microstructure.[34,46] This is because small homopolymers tend to distribute uniformly throughout the melt. Their nearly uniform distribution of A monomers, $\phi_{hA}(\mathbf{r})$, will produce a field with little spatial variation and thus with little tendency to induce segregation. They will instead dilute the copolymer concentration, effectly reducing χ just as a neutral solvent does, *i.e.*, the "dilution" approximation.[47]

Above, it was mentioned that large homopolymers lead to attractive interactions between micelles whereas small homopolymers lead to repulsive interactions.[13] Now we explain why this is so. Large homopolymers are relatively impenetrable to the corona of a micelle, and thus, the homopolymers see them as hard objects which restrict their configurational freedom. Consequently, the homopolymers tend to phase separate from the matrix between the micelles, reducing the spacing and producing an apparent attraction between micelles. On the other hand, considerable entropy of mixing is gained when small homopolymers pentrate the corona of a micelle. When the spacing between micelles increases, they overlap less, allowing more homopolymer in the corona and, therefore, increasing the entropy of mixing. This mechanism behaves equivalently to a repulsion between micelles.[15]

The entropy that drives the homopolymer from the middle of A-rich domains toward the interfaces is responsible for microstructural transitions that occur as ϕ increases.[21] In order to provide room for the homopolymer among the A blocks of the copolymer, the system makes a transition to a structure in which the interface is curved more toward the B-rich domains. One will notice that this is the same trend that occurs as f, the volume fraction of the A block, increases. Noticing this trend experimentally, refs 18 and 31 have correlated microstructure with the overall A-monomer volume fraction. Such an assumption is incorrect, because the mechanisms which drive the transitions as a result of increasing f and ϕ are quite different. Because the latter mechanism, which occurs when ϕ increases, originates from the entropy of mixing homopolymer with copolymer, it will be strongly influenced by α[22] and will become less important as the segregation increases.

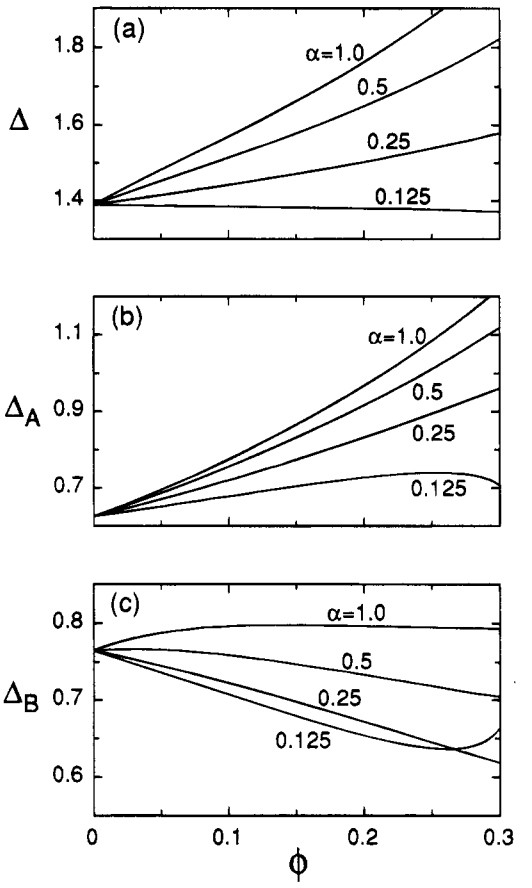

Figure 10. (a) Dimensionless lamellar spacing, $\Delta \equiv D/aN^{1/2}$, for an $f = 0.45$ diblock at $\chi N = 12$ as four different homopolymers are added. Dimensionless widths of the A-rich lamellae Δ_A and of the B-rich lamellae Δ_B are shown in (b) and (c), respectively.

Even when the tendency of the homopolymer to penetrate regions occupied by A blocks of the copolymer does not lead to a phase transition, it can, nevertheless, produce measurable effects on the dimensions of the microstructure. This occurs because the homopolymer spreads the copolymer molecules apart, increasing the interfacial area per copolymer. This, in turn, allows the B blocks of the copolymer to relax and the width of the B-rich domains to contract. For the lamellar phase, this effect has been carefully studied experimentally by Winey *et al.*[20] Our theoretical results reproduce much of the behavior they observed. First, in Figure 10a, we show the dimensionless period, $\Delta \equiv D/aN^{1/2}$, of the lamellar phase as homopolymer of various weights is added to a diblock melt. As found in experiment, when the molecular weight of the homopolymer is only somewhat less than that of the diblock, the period increases. However, low-weight homopolymer can cause the period to contract. A similar contraction has also been observed in triblock/homopolymer blends.[48] To understand what is happening, we decompose Δ into the dimensionless widths of the individual A- and B-rich lamellae, Δ_A and Δ_B, respectively. (For this calculation, we have defined the interfaces to occur at the inflection points in $\phi_A(z)$, *i.e.*, where its second derivative is zero.) The trends in Δ_A and Δ_B agree with the experimental results and are easily understood. A low-weight homopolymer has a high entropy of mixing and thus favors a broader distribution, as illustrated in Figure 9. Hence, it increases the interfacial area more than a high-weight homopolymer, producing a greater contraction in the B-rich lamellae. The lowest-weight ho-

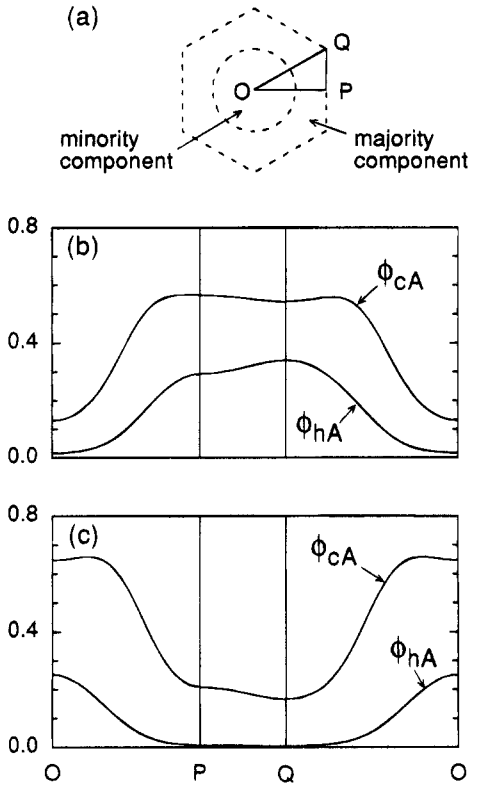

Figure 11. (a) Unit cell of the hexagonal phase showing the path O → P → Q → O. Along this path, the copolymer and homopolymer contributions to the A-monomer density, $\phi_{cA}(\mathbf{r})$ and $\phi_{hA}(\mathbf{r})$, respectively, are plotted for (b) $\chi N = 12$, $\alpha = 1$, $f = 0.59$, and $\phi = 0.20$ and for (c) $\chi N = 12$, $\alpha = 1$, $f = 0.39$, and $\phi = 0.05$.

mopolymer ($\alpha = 1/8$) has a distribution that is nearly uniform. As discussed above, this reduces the segregation in the melt and, in turn, causes the overall period to decrease. At $\phi \sim 0.2$, it even begins to disorder the melt, causing $\phi_A(\mathbf{r})$ to become sinusoidal and thus Δ_A and Δ_B to become equal.

The behavior discussed above is not unique to the lamellar phase but also occurs in other morphologies.[21,22] However, there is one effect expected for all the morphologies other than the lamellar one. The homopolymer will relieve some of the packing frustration that occurs from trying to fill space with units which prefer to be, for instance, cylindrical or spherical. Since flat layers can fill space, such frustration will not occur in the L phase. In the H phase, circular cylindrical units pack in a triangular lattice so as to efficiently fill space, but nevertheless, they cannot completely fill it. Without homopolymer, this must be done by deforming the units into the shape of a hexagon, but with homopolymer this is not necessary, as the homopolymer can fill the voids. In Figure 11a we show a hexagonal unit cell from the H phase. We have labeled three points in the cell. Point O is along the central axis of a cylinder, P is at the midpoint between two cylinders, and Q is in the middle of the region that causes the packing frustration. When homopolymer is added to the majority-component matrix, it tends to locate at Q so as to relieve the packing frustration imposed on the copolymer (see Figure 11b).

It is also informative to show what happens when homopolymer is added to the minority-component of the H phase (see Figure 11c). Here the homopolymer accumulates along the axis of the cylinder, swelling its radius and reducing the curvature of the interface. The analogous behavior will occur in the $Q_{Im\bar{3}m}$ and CPS phases where the basic unit prefers to be a sphere. In this way, the homopolymer makes the H, $Q_{Im\bar{3}m}$, and CPS phases accessible to the more symmetric copolymers. This counters the previous trend that results from the entropy of mixing. In the strong-segregation limit, where the latter effect becomes negligible, adding homopolymer to a minority component can drive the system to a microstructure with more curvature, *i.e.*, cylinders to spheres, or lamellae to cylinders.[13]

Although it is less clear where packing frustration occurs in the other more complex structures, presumably, the homopolymer reduces that stress in the same manner as for the H phase. Clearly, this is important between the L and H phases, where the more complicated structures compete for stability. We believe that it is this effect that brings about the two new equilibrium morphologies, the HPL and $Q_{Pn\bar{3}m}$ phases.

4. Summary

We have calculated the effect of blending A homopolymer with AB diblock copolymer. Our study has focused on weakly segregated blends. We first examined the phase coexistence between a diblock-rich microstructure and a homopolymer-rich disordered phase. There, we focused on a single diblock ($f = 0.45$) and restricted our attention to the lamellar microstructure. In our study, we found that the addition of high-weight homopolymer leads to macrophase separation between a diblock-rich lamellar phase and a homopolymer-rich disordered phase. This macrophase separation was attributed to an attractive interaction between diblock bilayers. However, low-weight homopolymer produced a repulsive interaction between bilayers, resulting in an entirely different behavior. Here, homopolymer could be added to the lamellar phase indefinitely without producing macrophase separation. Instead, the lamellar spacing diverged, leading to a continuous unbinding transition.

The highly swollen A-rich domains also occur in other microstructures. However, these regions are an artifact of the mean-field approximation because fluctuations would disorder the weakly bound superstructures, producing a fluctuation-induced order–disorder transition. We associate the disordered superstructures with the micellar regions present in real systems. The L, H, and CPS structures are expected to produce lamellar, cylindrical, and spherical micelles, respectively. We speculate that the HPL phase would produce disordered struts with most vertices being 3-fold coordinated. Each micellar region will become part of the disordered phase and the boundaries we calculated between them will no longer be true phase transitions. Still, these transitions can be used to delineate the different micellar regions. The unbinding transition is associated with a CMC line.

Within the A-rich domains of a microstructure, the A blocks of the copolymer are concentrated near the interface while the A homopolymer is preferentially located in the central region. Tension in the A blocks tends to push the homopolymer toward the middle of the A-rich domains, but this is countered by the entropy of mixing which favors a more uniform distribution of homopolymer. This latter effect is enhanced by lowering the molecular weight of the homopolymer. To allow homopolymer near the interface, the microstructure may undergo a phase transition to a geometry where the interface is curved less toward the A-rich domain. Even without a phase transition, homopolymer penetrates toward the interface by spreading apart the

diblocks and hence increasing the interfacial area. This has the interesting effect of allowing the B blocks to contract, thus reducing the thickness of the B-rich domains.

Perhaps the most important result in this study is that the homopolymer stabilizes new morphologies. These include the double-diamond, hexagonally-perforated lamellar, and close-packed spherical phases. We attribute this to the relief of packing frustration by the homopolymer. This effect may also stabilize other phases not considered in the present study. Because there is an endless number of possible structures, it is impossible to systematically consider them all. Experimental studies will be essential in determining whether additional structures occur in the diblock/homopolymer system.

Acknowledgment. We are grateful to F. S. Bates for the many conversations that contributed to this work. Financial support for this research was provided by the National Science Foundation through a grant (DMR 94-05101) to F. S. Bates and by the University of Minnesota Supercomputer Institute.

References and Notes

(1) Larsson, K. *J. Phys. Chem.* **1989**, *93*, 7304.
(2) Turner, D. C.; Wang, Z-G.; Gruner, S. M.; Mannock, D. A.; McElhaney, R. N. *J. Phys. II* **1992**, *2*, 2039.
(3) Seddon, J. M. *Biochim. Biophys. Acta* **1990**, *1031*, 1.
(4) Strey, R.; Schömacker, R.; Roux, D.; Nallet, F.; Olsson, U. *J. Chem. Soc., Faraday Trans.* **1990**, *86*, 2253.
(5) Fischer, S.; Fischer, H.; Diele, S.; Pelzl, G.; Jankowski, K.; Schmidt, R. R.; Vill, V. *Liq. Cryst.* **1994**, *17*, 855.
(6) Lindblom, G.; Rilfors, L. *Biochim. Biophys. Acta* **1989**, *988*, 221.
(7) Bates, F. S.; Schulz, M. F.; Khandpur, A. K.; Förster, S.; Rosedale, J. H.; Almdal, K.; Mortensen, K. *Faraday Discuss. Chem. Soc.*, in press.
(8) Whitmore, M. D.; Vavasour, J. D. *Macromolecules* **1993**, *26*, 7070. Matsen, M. W.; Schick, M. *Macromolecules* **1994**, *27*, 4014.
(9) Anderson, D. M.; Thomas, E. L. *Macromolecules* **1988**, *21*, 3221. Thomas, E. L.; Anderson, D. M.; Henkee, C. S.; Hoffman, D. *Nature* **1988**, *334*, 598.
(10) Hajduk, D. A.; Harper, P. E.; Gruner, S. M.; Honeker, C. C.; Thomas, E. L.; Fetters, L. J. *Macromolecules* **1995**, *28*, 2570.
(11) Schulz, M. F.; Bates, F. S.; Almda, K.; Mortensen, K. *Phys. Rev. Lett.* **1994**, *73*, 86. Hajduk, D. A.; Harper, P. E.; Gruner, S. M.; Honeker, C. C.; Kim, G.; Thomas, E. L.; Fetters, L. J. *Macromolecules* **1994**, *27*, 4063.
(12) Förster, S.; Khandpur, A. K.; Zhao, J.; Bates, F. S.; Hamley, I. W.; Ryan, A. J.; Bras, W. *Macromolecules* **1994**, *27*, 6922.
(13) Semenov, A. N. *Macromolecules* **1993**, *26*, 2273.
(14) Matsen, M. W. *Phys. Rev. Lett.* **1995**, *74*, 4225.
(15) Leibler, L.; Pincus, P. A. *Macromolecules* **1984**, *17*, 2922.
(16) McConnell, G. A. *Phys. Rev. Lett.* **1993**, *71*, 2102.
(17) Kinning, D. J.; Thomas, E. L.; Fetters, L. J. *J. Chem. Phys.* **1989**, *90*, 5806.
(18) Winey, K. I.; Thomas, E. L.; Fetters, L. J. *J. Chem. Phys.* **1991**, *95*, 9367.
(19) Koizumi, S.; Hasegawa, H.; Hashimoto, T. *Macromolecules* **1994**, *27*, 7893.
(20) Winey, K. I.; Thomas, E. L.; Fetters, L. J. *Macromolecules* **1991**, *24*, 6182.
(21) Tanaka, H.; Hasegawa, H.; Hashimoto, T. *Macromolecules* **1991**, *24*, 240.
(22) Hashimoto, T.; Tanaka, H.; Hasegawa, H. *Macromolecules* **1990**, *23*, 4378.
(23) Shull, K. R.; Mayes, A. M.; Russell, T. P. *Macromolecules* **1993**, *26*, 3929.
(24) Shull, K. R.; Winey, K. I. *Macromolecules* **1992**, *25*, 2637.
(25) Kinning, D. J.; Winey, K. I.; Thomas, E. L. *Macromolecules* **1988**, *21*, 3502.
(26) Mayes, A. M.; Olvera de la Cruz, M. *Macromolecules* **1988**, *21*, 2543.
(27) Kao, C. R.; Olvera de la Cruz, M. *J. Chem. Phys.* **1990**, *93*, 8284.
(28) Whitmore, M. D.; Noolandi, J. *Macromolecules* **1985**, *18*, 657. Whitmore, M. D.; Smith, T. W. *Macromolecules* **1994**, *27*, 4673.
(29) Disko, M. M.; Liang, K. S.; Behal, S. K.; Roe, R. J.; Joen, K. J. *Macromolecules* **1993**, *26*, 2983.
(30) Hashimoto, T.; Koizumi, S.; Hasegawa, H.; Izumitani, T.; Hyde, S. T. *Macromolecules* **1992**, *25*, 1433.
(31) Winey, K. I.; Thomas, E. L.; Fetters, L. J. *J. Chem. Phys.* **1992**, *25*, 422.
(32) Spontak, R. J.; Smith, S. D.; Ashraf, A. *Macromolecules* **1993**, *26*, 956.
(33) Samples earlier identified as $Q_{Pn\bar{3}m}$ in refs 18 and 31 have now been reexamined and assigned to the $Q_{Ia\bar{3}d}$ morphology. Hajduk, D. A. Private communication.
(34) Whitmore, M. D.; Noolandi, J. *Macromolecules* **1985**, *18*, 2486.
(35) Whitmore, M. D.; Vavasour, J. D. *Acta Polym.*, in press.
(36) Helfand, E. *J. Chem. Phys.* **1975**, *62*, 999.
(37) Matsen, M. W.; Schick, M. *Phys. Rev. Lett.* **1994**, *72*, 2660.
(38) The generalization where A and B monomers have unequal segment lengths is straightforward as illustrated in ref 8.
(39) *International Tables for X-Ray Crystallography*; Henry, N. F. M., Lonsdale, K., Eds.; Kynoch: Birmingham, U. K., 1969.
(40) The 2-dimensional space group for the H phase is no. 17. The space groups for the triply-periodic phases examined in this paper are no. 166 (abcabc... HPL), 194 (abab... HPL, and hcp CPS), 221 (sc spheres), 224 ($Q_{Pn\bar{3}m}$), 225 (fcc CPS), 229 ($Q_{Im\bar{3}m}$), and 230 ($Q_{Ia\bar{3}d}$).
(41) Hong, K. M.; Noolandi, J. *Macromolecules* **1981**, *14*, 727.
(42) Banaszak, M.; Whitmore, M. D. *Macromolecules* **1992**, *25*, 249. Hong, K. M.; Noolandi, J. *Macromolecules* **1983**, *16*, 1083.
(43) Fredrickson, G. H.; Helfand, E. *J. Chem. Phys.* **1987**, *87*, 697. Muthukumar, M. *Macromolecules* **1993**, *26*, 5259.
(44) Shull, K. R. Macromolecules **1993**, *26*, 2346.
(45) Han, D. H.; Baek, D. M.; Kim, J.; Kimishima, K.; Hashimoto, T. *Macromolecules* **1992**, *25*, 3052.
(46) Olvera de la Cruz, M.; Sanchez, I. C. *Macromolecules* **1987**, *20*, 440.
(47) Fredrickson, G. H.; Leibler, L. *Macromolecules* **1989**, *22*, 1238.
(48) Quan, X.; Gancarz, I.; Koberstein, J. T.; Wignall, G. D. *Macromolecules* **1987**, *20*, 1431.

MA950456E